Evaluation of undrained failure envelopes of caisson foundations under combined loading

Moura Mehravar (corresponding author), PhD, MSc, BSc

Wolfson School of Mechanical and Manufacturing Engineering
Loughborough University
Leicestershire, United Kingdom
LE11 3TU
E-mail: M.Mehravar@lboro.ac.uk

Ouahid Harireche, PhD, MSc, BSc

Islamic University in Madinah, KSA
Faculty of engineering
Department of civil engineering
E-mail: O.Harireche@gmail.ac.uk

Asaad Faramarzi, PhD, MSc, BSc

School of Civil Engineering,
The University of Birmingham
Edgbaston, Birmingham B15 2TT, United Kingdom
Tel: +44 (0) 121 414 5050
E-mail: A.Faramarzi@bham.ac.uk

Evaluation of undrained failure envelopes of caisson foundations under combined loading

Abstract

In this paper, results of a three-dimensional finite element study addressing the effect of embedment ratio (L/D) of caisson foundations on the undrained bearing capacity under uniaxial and combined loadings are discussed. The undrained response of caisson foundations under uniaxial vertical (*V*), horizontal (*H*) and moment (*M*) loading are investigated. A series of equations are proposed to predict the ultimate vertical, moment and maximum horizontal bearing capacity factors. The undrained response of caisson foundations under combined *V-H* and *V-M* load space is studied and presented using failure envelopes generated with side-swipe method. The kinematic mechanism accompanying failure under uniaxial loading is addressed and presented for different embedment ratios. Predictions of the uniaxial bearing capacities are compared with other models and it is confirmed that the proposed equations appropriately describe the capacity of caisson foundations under uniaxial vertical, horizontal and moment loading in homogenous undrained soils. The results of this paper can be used as a basis for standard design codes of off-shore skirted shallow foundations which will be the first of its kind.

Keywords: bearing capacity; caisson; shallow foundation; three-dimensional finite element modelling; undrained analysis.

1 Introduction

A suction caisson consists of a thin-walled upturned ‘bucket’ of cylindrical shape made from steel. This type of foundation has proven to be efficient and versatile as a support for offshore structures and appears to be a very attractive option for future use in offshore wind turbines [1-4]. The thin caisson wall facilitates installation when a pressure differential is induced by suction on the caisson lid, which pushes the caisson to penetrate into the seabed. This is achieved by pumping out the water trapped in the caisson cavity after initial penetration under self-weight [5-8]. The skirt can improve the foundation bearing capacity by trapping the soil between them during undrained loading [9-10]. A number of studies have been conducted on the investigation of bearing capacities of caisson foundations. However, in the most of the former studies the foundation was either analysed as a skirted strip foundation using finite element analyses (FEA) and upper bound solutions or as a surface circular foundation using three-dimensional FEA without considering the skirt length in the simulation [11-20]. On the other hand, offshore foundations are three-dimensional and embedded. The skirt length has a considerable impact on their bearing capacities. Only few studies were performed by considering the caisson foundation using three-dimensional model. Most of these analyses did not comprehensively covered a wide range of practical embedment ratios or investigate all vertical, horizontal and moment bearing capacities [21-22]. A summary of previous studies on undrained bearing capacities and failure envelopes of shallow foundations are presented in Table 1.

Table 1

In the present study the main objective is to perform three-dimensional (3D) undrained numerical simulations to predict the bearing capacity of caisson foundations under uniaxial and combined loading conditions. The present study refers mainly to the work done by Gourvernec [18], Bransby and Randolph [11], which are essentially plane strain analyses. It has been justified that within such context, the assumption of full bonding between the caisson and surrounding soil is plausible (especially that suction development at the interface in undrained condition prevents separation). Hence, the work performed in the current paper has been limited to a similar context, taking advantage of efficient numerical computations and reasonable computational time. An extension of the present work by implementing interfaces would shed more light on the accuracy of both plane strain and 3D models, but such an extension is beyond the scope of the present paper.

In this paper, a series of three-dimensional finite element analyses using ABAQUS [23] are performed to investigate the effect of the embedment depth on the bearing capacity of shallow foundations in homogenous undrained soil. Different aspect ratios of caisson foundation "L/D = 0, 0.25, 0.5, 0.75, 1", where L is the embedment length and D is the caisson diameter are considered. Uniaxial vertical (V), horizontal (H) and moment (M) bearing capacities are investigated and presented as a series of equations to estimate the uniaxial ultimate vertical, moment and maximum horizontal bearing capacity factors of caisson foundations. Finally, the capacities of caisson foundations under combined *VH*, *VM* load space are studied and expressed by failure envelopes.

2 Numerical modelling

2.1 Model geometry and mesh

In order to obtain precise results, a series of three-dimensional finite element analyses were carried out for the practical range of embedment ratios, $L/D = 0$ (surface foundation), 0.25, 0.5, 0.75 and 1 in a homogenous undrained soil profile. It is important to cover a wide range of values starting from the special case of a surface foundation and moving towards moderately deep foundations ($L/D \leq 1$). However, the number of aspect ratio investigated has been kept to a reasonable maximum to keep the simulation concise and comprehensive.

Taking advantage of the symmetrical nature of the problem, only half of the entire system was modelled. Figure 1 shows a semi-cylindrical section through a diametrical plane of a caisson foundation with $L/D=0.5$. This figure also represents the typical finite element mesh for caisson foundation, used in this study. A number of different mesh densities in which element sizes around the caisson wall and tip are considerably refined were performed to obtain accurate results in a reasonable computational time. The mesh is extended 5D from the caisson foundation centre line and top of the soil, respectively so that the failure loads are not sensitive by their position or to the boundary conditions. The caisson thickness is considered 4×10^{-3} D, which reflects a reasonable value for typical caisson foundations. Displacements in all three coordinate directions (x, y and z) at the bottom of the base of the mesh were completely fixed, and also normal displacements on the lateral boundaries were prevented.

Figure 1

The caisson foundation nomenclature and the sign convention which is adopted in this study are presented in Figure 2.

Figure 2

In order to model the soil, first-order, eight-node linear brick, reduced integration continuum with hybrid formulation element (C3D8RH) is employed. The hybrid elements are appropriate to model the behaviour of near-incompressible materials such as undrained soils [18].

2.2 Material modelling

In this study the soil is modelled as a linear elastic-perfectly plastic material based on the Tresca failure criterion ($\varphi = 0^o$) with an effective unit weight $\gamma' = 6 \mathrm{kN/m}^3$ and Poison's ratio $\nu = 0.49$. The undrained shear strength of the clay are considered as $S_u = 5\mathrm{kPa}$ with an undrained young's modulus to undrained shear strength ratio (E_u / S_u) of 500. The foundations are modelled physically as rigid bodies with a Young's modulus of $E = 10^9 E_u$ and $\gamma = 78 \mathrm{~kN/m}^3$. The interface between soil and foundation was fully bonded so that there is no detachment between the soil and the foundation [13]. This assumption for interface is particularly relevant to caisson foundations since they have a significant uplift capacity, especially for short term loading [11] and the developed suction at the interface prevents separation in undrained condition. A tensile resistance develops at the foundation level under undrained loading condition due to suction pressure within the soil plug.

2.3 Loading path

In this study the loading is applied using a displacement-controlled method by prescribing vertical (w), horizontal translation (u) or rotation (θ) at the reference point RP (Figure 2). It should be mentioned that, due to the capability to predict post-failure conditions, the displacement-controlled method, is more appropriate than the stress-controlled method for achieving failure loads [14, 24-25]. In order to obtain failure envelopes in *V-H* and *V-M* spaces the so-called "side-swipe" test is performed. This method was firstly used by Tan [26] during his centrifuge test, and consists of two stages. Initially, a given displacement at one direction (typically vertical) is applied to the foundation until bringing the foundation to the failure condition. In the second stage, displacement in other degrees of freedom is prescribed whilst the vertical displacement increment is set to zero and the foundation is "swiped" either horizontally or in rotation. The stress path in the second stage can almost define the shape of the failure envelope because the elastic stiffness is much larger than the plastic stiffness. Advantageously, this method is able to determine a large section of the failure envelope in a single test.

3 Finite element analysis results

3.1 Vertical bearing capacity

Firstly, it should be mentioned that to achieve results which can be applied to any caisson geometry and undrained soil strength the obtained data from this study are normalised with respect to the foundation diameter (D) and undrained soil strength (S_u). Figure 3 and Figure 4 show the predicted variation of normalised vertical load versus normalised vertical displacement (w/D) and the vertical bearing capacity factor ($N_{cv} = F_v/A.S_u$, in which A is area of the caisson horizontal cross section) as a function of various embedment ratios (L/D), respectively.

Figure 3

Figure 4

Figure 4 shows that the vertical bearing capacity increased non-linearly by increasing the embedment ratio. This confirms the effect of the skirt length in enhancing the vertical bearing capacity of caisson foundations. However, a smaller rate of the increasing trend is observed for $L/D \geq 0.7$. This phenomenon can be explained as being due to the changing failure mechanism for an increasing skirt length form the traditional Prandtl theory of surface foundations (Figure 5a), and such a mechanism switch to a confined failure mechanism for a long skirt (Figure 5b).

Figure 5 (a-b)

Based on the three-dimensional finite element results obtained from this study, a quadratic relationship is proposed to predict the vertical capacity depth factor

$d_{cv} = N_{cv(\frac{L}{D})} \Big/ N_{cv(\frac{L}{D}=0)}$ of caisson foundations (Figure 6), in which $N_{cv(\frac{L}{D}=0)} = 6.2$. It should be mentioned that this proposed equation is valid only for an embedment ratio range, $0 \le L/\mathrm{D} \le 1$. For embedment ratios beyond this range the equation should be applied with care and further simulations are required.

$$d_{cv} = -0.28\left(\frac{L}{D}\right)^2 + \left(\frac{L}{D}\right) + 1 \qquad (1)$$

Figure 6

3.1.1 ***Comparing vertical bearing capacity with other published data***

The results for vertical bearing capacity factors are compared with other published data. For the circular surface foundation (L/D=0), a vertical bearing capacity factor $N_{cv} = 6.2$ was obtained which represents an overestimation of 2.5% compared to the exact solutions of $V_{ult} = 6.05\ A.S_u$ [27-29]. Table 2 presents a brief comparison between the vertical bearing capacity factors of circular surface foundation proposed by different approaches.

Table 2

It should be highlighted that exact solutions of the vertical bearing capacity of skirted strip or embedded three-dimensional foundations are not available. However, for comparison, an upper bound solution for a fully rough, embedded strip foundation has been obtained by Bransby and Randolph [11], and Plane-strain finite element results for fully rough caisson foundations have been conducted by Gourvenec [18]. A prediction from the conventional vertical depth factor [30] is also presented in Figure 7.

Figure 7

It can be seen from Figure **7** that the values of the undrained vertical bearing capacity of caisson foundation based on Skempton's depth factor are considerably small compared to the prediction by either this study or other published data for a rough foundation. For instance, the conventional Skempton's method underestimated the amount of vertical bearing capacity by more than a 45% for L/D = 0.5. Indeed, although conventional depth factors have been applied to rough and smooth, circular and strip foundations, they have been originally suggested for smooth-sided circular foundations [18]. In other words, the bearing capacity predicted by the conventional method does not consider the contribution of the friction between skirt and soil.

Additionally, a comparison between this study and a finite element analysis performed by Gourvenec [18] indicates that, using a plane-strain analysis for caisson foundation underestimates the vertical bearing capacity factor (e.g about 17% for L/D = 1). This difference can be explained by the fact that in a 2D analysis, the effects of foundation shape and soil-structure interaction are not considered properly. Meanwhile, a three-dimensional analysis allows the additional soil deformation mechanism to be taken into consideration.

The upper bound solution by Bransby and Randolph [11] also underestimates the actual bearing capacity. Because the caisson foundation was described using a two-dimensional model. It should be also noted that since in the upper bound solution, the effect of an increasing embedment ratio (*L*/D) on the failure mechanism has not been considered, the linear increasing trend of vertical bearing capacity is not beyond the expectation.

3.2 Maximum horizontal bearing capacity

Figure 8 and Figure 9 present the normalised results of the variation of maximum horizontal load ($F_{h\ (max)}$) against horizontal displacement ratio (u/D) and the maximum horizontal bearing capacity factor ($N_{ch\ (max)} = F_{h\ (max)} / A.S_u$) as a function of various embedment ratios (*L*/D), respectively. In this section the maximum horizontal loads and bearing capacity correspond to pure horizontal translation ($u > 0$ and θ is constrained).

Figure 8

Figure 9

In contrast with the nonlinear smooth increasing trend for $L/D \geq 0.7$ which was observed for the ultimate vertical bearing capacity factor of caisson foundations, Figure 9 revealed that maximum horizontal bearing capacity increasing rate with an increasing embedment ratio (L/D) is linear. The main reason is, when rotation is constrained and pure horizontal translation is applied, no coupling between rotation and horizontal degree of freedom develops. Hence, a pure sliding mechanism occurs for all embedment ratios.

Figure 10 (a-d) show the failure mechanism under pure horizontal translation using incremental displacement vectors for different embedment ratios.

Figure 10(a-d)

Based on these results a linear relationship can be expressed to explain the maximum horizontal depth factor $d_{ch(\max)} = N_{ch(\max)\left(\frac{L}{D}\right)} \Big/ N_{ch(\max)\left(\frac{L}{D}=0\right)}$ for the embedment ratios up to unity, where $N_{ch(\max)\left(\frac{L}{D}=0\right)} = 1$.

$$d_{ch(\max)} = 7.5\left(\frac{L}{D}\right) + 1 \tag{2}$$

Figure 11

3.2.1 *Comparing horizontal bearing capacity with other published data*

The calculated results for maximum horizontal bearing capacity factor by Gourvenec [18] and Bransby and Randolph [11] are shown in Figure 12, and are compared to the obtained result in this study.

Figure 12

Figure 12 indicates that all above predictions for $N_{ch\ (max)}$ show a linear increasing trend for embedment ratios up to unity. However, both predictions by Gourvenec [18] and Bransby and Randolph [11] of the maximum horizontal bearing capacity of caisson foundation based on Plane-strain and upper bound solution respectively, underestimated the bearing capacity. The main reason is that in both cases, the problem was considered as two dimensional. Hence, the effect of foundation shape was not reflected in their predictions.

Furthermore, in order to demonstrate the effect of kinematic failure mechanism on the horizontal capacity of embedded foundations, the ultimate horizontal bearing capacity obtained through a three-dimensional finite element analysis under pure horizontal load by Hung and Kim [21] is presented and compared with the calculated maximum horizontal bearing capacity obtained in this study by applying pure sliding (Figure 13). It should be noted that the ultimate bearing capacity (subscripted by ‘ult’) corresponds to the pure horizontal load ($\theta \neq 0$).

Figure 13

It can be observed from Figure 13 that there is a non-linear increasing rate of ultimate horizontal bearing capacity which is smaller for $0.25 \leq L/\mathrm{D} \leq 0.5$, while the maximum horizontal bearing capacity increases linearly. The main reason can be explained by the difference between the failure mechanisms in maximum and ultimate horizontal bearing capacities. Indeed, when pure horizontal translation is applied to the foundation level, there is no coupling between horizontal and rotation degrees of freedom and the pure sliding mechanism governs failure, while under pure horizontal loading condition, there exists a coupling between horizontal and rotation degrees of freedom, which can cause both horizontal and rotation displacements. Additionally, under pure horizontal loading when $0.25 \leq L/\mathrm{D} \leq 0.5$ no coupling between horizontal and rotation degree of freedom was observed by [21], therefore the difference between the ultimate and maximum horizontal bearing capacity is small (Figure 13).

In addition, it can be clearly observed that, for $L/\mathrm{D} \geq 0.75$ the difference between ultimate and maximum horizontal bearing capacities becomes more significant. This indicates that under pure horizontal loading the effect of coupling becomes more considerable with an increasing embedment ratio (L/D), since the failure mechanism activates more rotation and less sliding. Consequently, the three-dimensional finite element analysis confirms that by constraining the rotation degree of freedom ($\theta = 0$) of a caisson foundation, horizontal bearing capacity can be enhanced (e.g. about 46% for L/D=1).

3.3 Ultimate moment bearing capacity

Figure 14 and Figure 15 present the normalised results of the variation of ultimate moment load (M_{ult}) against normalised rotational degree of freedom (θ/D) and the ultimate moment capacity as a function of various embedment ratios (L/D), respectively. It should be mentioned that in this section ultimate moment load and capacity correspond to the pure moment load ($\theta > 0$ and u is not constrained), which means that when a pure moment is applied at foundation level, both rotation and horizontal degrees of freedom affect the failure mechanism.

Figure 14

Figure 15

These figures reveal that by increasing the embedment ratio, the ultimate bearing capacity of the caisson foundations increases non-linearly. However, for embedment ratios (L/D) $\geq$ 0.75, the increasing rate of ultimate moment capacity decreases. This can be justified by the fact that at larger embedment depth, the effect of coupling between horizontal and rotational degrees of freedom becomes more discernible. Indeed, at larger embedment depths, more sliding and less rotation accompany the failure mechanism. Figure 16 (a-d) shows the failure mechanism under pure moment load by incremental displacement vectors for various embedment ratios.

Figure 16(a-d)

The scoop mechanism can be detected from Figure 16(a-d) for the failure mechanism under pure moment load, in which there exists a clear distance between the rotation centre and the foundation tip. In addition, by increasing the embedment length, the centre of rotation tends to move towards the foundation level.

Based on these obtained results the following quadratic equation is proposed to express the ultimate moment capacity depth factor $d_{ch(ult)} = N_{ch(ult)(\frac{L}{D})} \Big/ N_{ch(ult)(\frac{L}{D}=0)}$, in which $N_{ch(ult)(\frac{L}{D}=0)} = 0.55$.

$$d_{cm(ult)} = -0.37\left(\frac{L}{D}\right)^2 + 2.54\left(\frac{L}{D}\right) + 1 \tag{3}$$

Figure 17

3.3.1 *Comparison of the ultimate moment bearing capacity with other published data*

The calculated results for the ultimate moment bearing capacity factor by Gourvenec [18] and Bransby and Randolph [11] are presented in Figure 18. These results are compared to the three-dimensional finite element predictions performed in this study.

Figure 18

It can be observed from Figure 18 that for embedment ratios less than 0.5 there is no significant difference between the predicted results by this study and those achieved with a plane-strain finite element analysis [18]. A similar observation can be made regarding the comparison with the upper bound by Bransby and Randolph [11]. This later solution is based on a cylindrical scoop cutting the edge of the foundation.

However, the difference becomes more pronounced as the embedment ratio increases (e.g. L/D > 0.7).This discrepancy reflects the fact that a three-dimensional analysis takes into account the foundation shape, which is ignored in the two-dimensional model. In fact, the effect of foundation shape clearly indicates that by increasing the embedment ratios (e.g. L/D ≥ 0.7) the increasing rate of ultimate moment capacity decreases due to the effect of coupling between rotation and horizontal degrees of freedom. Hence, for larger embedment ratios, more sliding and less rotation govern the failure mechanism Figure 16(a-d).

3.4 Failure envelopes

Failure envelopes provide a practical way to visualise the behaviour of foundations under combined loading conditions. For loading conditions inside the envelope, the foundation response is elastic. The boundary of the envelope corresponds to the yielding of the foundation. Mainly, side-swipe test and constant displacement method which are both based on displacement control have been used by various researchers to capture the shape of the yield-locus. In this study, side-swipe method is employed to obtain failure envelopes under combined vertical-horizontal and vertical- moment loading conditions.

As it was mentioned in section 2.3 this method was used for the first time by Tan [26]. The first and second stages of the side-swipe method are shown in Figure 19 by probes AB and BC respectively. Probe AB is obtained by prescribing a given displacement (typically vertical) to the foundation until the ultimate load is reached. At the next stage, indicated by the probe BC in Figure 19 a second displacement (horizontal or rotational) is prescribed to the foundation while the vertical displacement increment is set to zero.

Figure 19

3.4.1 ***Combined horizontal and vertical loading (zero moment load)***

Figure 20 show the obtained failure envelopes under combined vertical and horizontal loading conditions for different embedment ratios (*L*/D=0, 0.25, 0.5, 0.75, 1), respectively. It is clear that there is no difference between the shapes of the failure envelopes for all embedment depths. However, by increasing embedment ratios the failure envelopes expand, which confirms the effect of the embedment depth on increasing the load carrying capacity. On the other hand, this expanding rate decreases for embedment ratios beyond 0.75 roughly. It can be also seen that in the presence of horizontal loading, the vertical bearing capacity factor (N_{cv}) decreases.

Figure 20

3.4.2 *Combined vertical and moment loading (zero horizontal load)*

Figure 21 illustrate the failure envelopes under combined vertical-moment loading of caisson foundations for different embedment ratios *L*/D = 0, 0.25, 0.5, 0.75 and 1. These figures indicate that, despite their similar shape, the failure envelopes have a size that expands for an increasing embedment ratio (*L*/D). However, for *L*/D ≥ 0.75 this expanding rate decreases. This phenomenon confirms the efficiency of using caisson foundations compared with shallow surface foundation to enhance vertical-moment bearing capacity. Figure 21 also reveals that decreasing in moment loading accompanying utilisation the ultimate vertical capacity.

Figure 21

4 Conclusion

In this paper a series of three-dimensional finite element analyses have been conducted with ABAQUS in order to evaluate the uniaxial undrained bearing capacity factors as well as to obtain failure envelopes in the *V-H* and *V-M* spaces for caisson foundations at various embedment ratios ((*L*/D)= 0, 0.25, 0.5, 0.75, 1). Based on the simulation results three individual equations have been proposed for the ultimate vertical and moment as well as maximum horizontal depth factor. Additionally, the results of uniaxial bearing capacity factors were compared with proposed solutions and obtained results by other studies.

An increasing trend was observed in the value of the ultimate vertical bearing capacity factor for an increasing embedment ratio. However, the results (Fig 4 and Fig 6) indicate that such an increase is less pronounced for *L*/D ≥ 0.7, due to the transition of the failure mechanism as it was illustrated in Fig 5(a-b).

On the other hand, the maximum horizontal bearing capacity is found to increase linearly for embedment ratios up to unity. The numerical simulations revealed that under pure horizontal translation, a pure sliding mechanism governs failure. Moreover, the maximum horizontal bearing capacities were compared with the ultimate horizontal capacity of caisson foundations and have indicated that constraining the rotation degree of freedom causes an improvement in the horizontal bearing capacity of caisson foundations.

The results have shown that the rate of ultimate moment capacity decreases for embedment ratios (L/D) ≥ 0.75, which can be explained to be due to the fact that at larger embedment depths, more sliding and less rotation accompanies the failure mechanism.

Moreover, the failure mechanism under maximum horizontal load and ultimate moment and vertical loading were investigated for different embedment ratios (L/D). Under ultimate moment loads (when the horizontal displacement is not constrained), scoop mechanism was observed with a centre point that lies above the caisson tip, but moves towards it for an increasing embedment ratio. The results achieved in this paper can be used as a basis for standard design codes of off-shore skirted shallow foundations which will be the first of its kind. For all mentioned embedment ratios, side-swipe tests were conducted to obtain yield loci as well as failure envelopes in V-H and V-M spaces and similar shapes were observed. The results indicated that the failure envelopes expand for an increasing embedment ratio, in which the expansion rate for approximately $L/D \geq 0.75$ decreased.

References:

[1] Tjelta, T. I. & Haaland, G., 1993. Novel foundation concept for a jacket finding its place. *Offshore site investigation and foundation behaviour,* Volume 28, pp. 717-728.

[2] Byrne, B. W., Houlsby, G. T., Martin, C. & Fish, P., 2002. Suction caisson foundations for offshore wind turbines. *Wind Enineering,* 26(3), pp. 145-155.

[3] Byrne, B. W. & Houlsby, G. T., 2003. Foundation for offshore wind turbines. *Philosophical Transactions of the Royal Society of London*, 361(Series A), pp. 2909-2930.

[4] Luke, A. M., Rauch, A. F., Olson, R. E. & Mecham, E. C., 2005. Componenet of suction caisson capacity measured in axial pullout tests. *Ocean Engineering,* Volume 32, pp. 878-891.

[5] Houlsby, G. T. & Byrne, B. W., 2005. Design procedures for installation of suction caissons in sand. *Proceedings of the Institution of Civil Engineers, Geotechnical Engineering,* 158(GE3), pp. 135-144.

[6] Harireche, O., Mehravar, M. & Alani, A. M., 2013. Suction caisson in stallation in sand with isotropic permeability varying with depth. *Applied Ocean Research,* Volume 43, pp. 256-263.

[7] Harireche, O., Mehravar, M. & Alani, A. M., 2014. Soil conditions and bounds to suction during the installation of caisson foundations in sand. *Ocean Engineering,* Volume 88, pp. 164-173.

[8] Mehravar, M., Harireche, O., Faramarzi, A., Alani, A.M. 2015. Modelling the Variation of suction pressure during caisson installation in sand using FLAC3D. *Ships and Offshore Structures*, pp. 1-7.

[9] Tani, K. & Craig, W. H., 1995. Bearing capacity of circular foundations on soft clay of strength increasing with depth. *Soils Found,* 35(4), pp. 21-35.

[10] Bransby, M. F. & Randolph, M. F., 1998. Combined loading of skirted foundations. *Geotechnique,* 48(5), pp. 637-655.

[11] Bransby, M. F. & Randolph, M. F., 1999. The effect of embedment depth on the undrained response of skirted foundations to combined loading. *Soil and Foundations,* 39(4), pp. 19-33.

[12] Gourvenec, S. & Barnett, S., 2011. Undrained failure envelope for skirted foundations under general loading. *Geotechnique*, 61(3), pp. 263-270.

[13] Bransby, M. F. & Yun, G. J., 2009. The undrained capacity of skirted strip foundations under combined loading. *Geotechnique,* 59(2), pp. 115-125.

[14] Gourvenec, S. & Randolph, M., 2003. Effect of non-homogeneity on the shape of failure envelopes for combined loading of strip and circular foundations on clay. *Geotechnique,* 53(6), pp. 575-586.

[15] Randolph, M. F.,& Puzrin, A. M., 2003. Upper bound limit analysis of circular foundations on clay under general loading. *Geotechnique* **53**, No. 9, 785-796.

[16] Gourvenec, S. (2007). Failure envelopes for offshore shallow foundations under general loading. *Geotechnique* **57**, No. 3, 715-728.

[17] Yun, G & Bransby, M. F., 2007. The undrained vertical bearing capacity of skirted foundations, *Soils and Found*, Vol 47, No 3, pp 493-505

[18] Gourvenec, S., 2008. Effect of embedment on the undrained capacity of shallow foundations under general loading. *Geothechnique,* 58(3), pp. 177-185.

[19] Taiebat, H. A. & Carter, J. P., 2010. A failure surface for shallow circular footing on cohesive soils. *Geothechnique* **60**, No. 4, 256-273.

[20] Sukumaran, B., McCarron, W. O., JeanJean, P. & Abouseeda, H., 1999. Efficient finite element techniques for limit analysis of suction caissons under lateral loads. *Computers and Geptechnics,* Volume 24, pp. 89-107.

[21] Hung, L. C. & Kim, S. R., 2012. Evaluation of vertical and horizental bearing capacities of bucket foundations in clay. *Ocean Engineering,* Volume 52, pp. 75-82.

[22] Vulpe, C., Gourvenec, S. & Power, M., 2014. A generalised failure envelope for undrained capacity of circular shallow foundations under general loading. *Goetechnique letter,* Volume 4, pp. 187-196.

[23] Simulia, 2012. *ABAQUS usser's manua. Dassault Systemes Simula Crop.*

[24] Houlsby, G. T. Martin, C. M., 2003. Undrained bearing capacity factors for conical footings on clay. *Geotechnique*, 53(5), pp. 513-520.

[25] Bransby, M. F. & Randolph, M. F., 1997. Shallow foundations subject to combined loading. Wuhan, *Proceeding of the 9th international conference on computer methods in advanceds in geomechanics*.

[26] Tan, F. S., 1990. Centrifuge and theoretical modelling of conical footing on sand, Cambridge: PhD thesis, University of Cambridge.

[27] Cox, A. D., Eason, G. & Hopkins, H. G., 1961. Axially symmetric plastic deformation in soils. *Philosofical Transaction of the Royal Society London,* 254(1036), pp. 1-45.

[28] Houlsby, G. T. & Wroth, C. P., 1983. Calculation of sressses on shallow petrometers and footings. Newcastle, *Proceedings of IUTAM/IUGG seabed Mechanics.*

[29] Martin, C. M., 2001. Vertical bearing capacity of skirted circular foundations on Tresca soil. Istanbul, *Proceeding of 15th International Conference on Soil Mechanics and Geotehcnical Engineering.*

[30] Skempton, A. W., 1951. The beraring capacity of clays. London, *Proceedings of Building Research Congress.*

[31] Houlsby, G. T., Kelly, R. B., Huxtable, J. & Byrne, B. W., 2005. Field trials of suction caissons in clay for offshore wind turbine foundations. *Geotechnique,* 55(4), pp. 287-296.

List of Tables:

List of Figures:

Figure 13: A comparison between ultimate and maximum horizontal bearing capacity factors; $N_{ch\ (ult)}$ & $N_{ch\ (max)}$ when θ *is* constrained

Figure 14: Normalised moment for different embedment ratios (*L*/D) vs normalised rotation (θ/D)

Figure 15: Ultimate moment capacity as a function of embedment ratio

Figure 16 (a-d): Failure mechanism under moment load (M_{ult}; *u* is not constrained), (a) *L*/D=0.25, (b) *L*/D=0.5, (c) *L*/D=0.75, (d) *L*/D=1

Figure 17: Ultimate moment capacity depth factor as a function of L/D ratios

Figure 18: Comparison of ultimate moment bearing capacity factor

Figure 19: A cross section of yield locus in V-H space using side-swipe method

Figure 20: Failure envelopes for vertical and horizontal loading space (moment load = 0)

Figure 21: Failure envelopes for vertical and moment loading space (horizontal load = 0)

Table

Table 1: A summary of studies on undrained bearing capacities of shallow foundation

Footing Geometry	**Embedment**		**Investigated capacity**	**Method**	**Reference**
	Surface	**Embedded**			
Strip	√	_	*VHM*	FEM	Bransby & Randolph (1998)
Strip	_	√	*VHM*	FEM/UB	Bransby & Randolph (1999)
Strip, Circular	√	_	*VHM*	FEM	Gourvenec & Randolph (2003)
Circular	√	_	*VHM*	LUB	Randolph & Puzrin (2003)
Circular	√	_	*VHM*	FEM	Gourvenec (2007)
Strip	√	√	*V*	FEM/UB	Yun & Bransby (2007)
Strip	√	√	*VHM*	FEM	Gourvenec (2008)
Strip	_	√	*HM*	FEM/UB	Bransby & Yun (2009)
Circular	√	_	*VHM*	FEM	Taiebat & Carter (2010)
Circular	√	(L/D≤1)	*VH*	FEM	Hung & Kim (2012)
Circular	√	(L/D≤0.5)	*VHM*	FEM	Vulpe et al. (2014)
Circular	√	(0≤L/D≤1)	*VHM*	FEM	This study

Table 2: Comparison with published data for N_{cv} of circle surface foundation

	Method	**N_{cv}**
This study	3D Finite element results	6.2
Gourvenec, 2008	2D Finite element results	5.21
Gourvenec and Randolph, 2003	3D Finite element results	5.91
Cox et al., 1961	Exact solution	6.05
Houlsby and Wroth, 1983		6.05
Martin, 2001		6.05

Figure

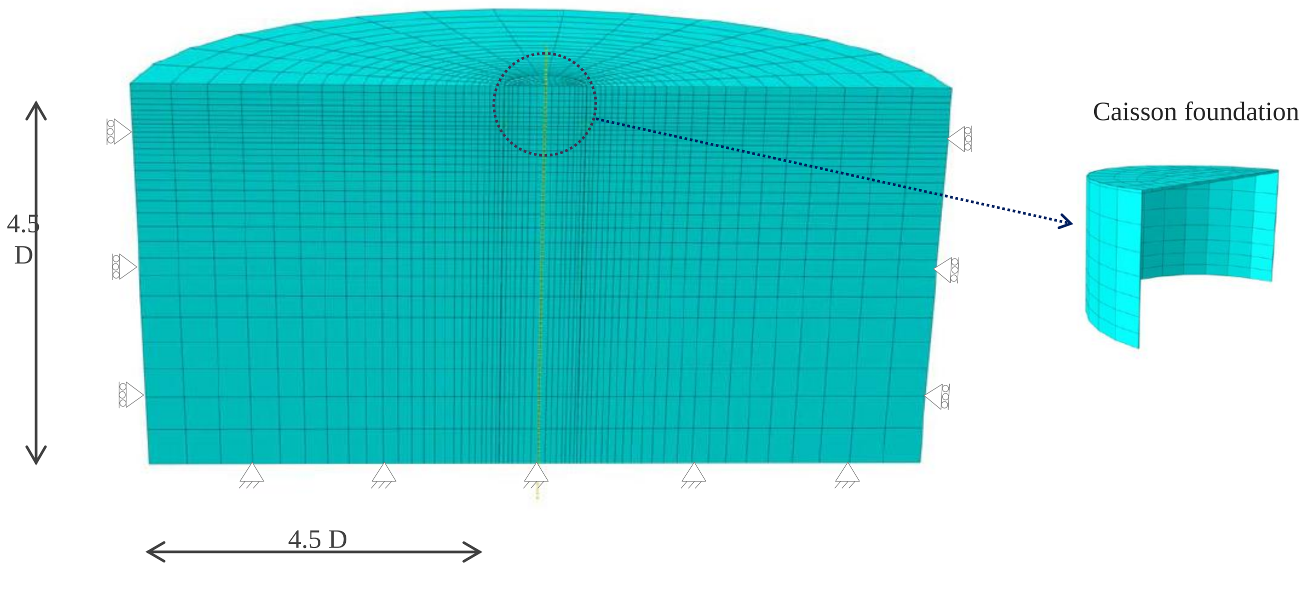

Figure 1: Finite element mesh and boundary conditions

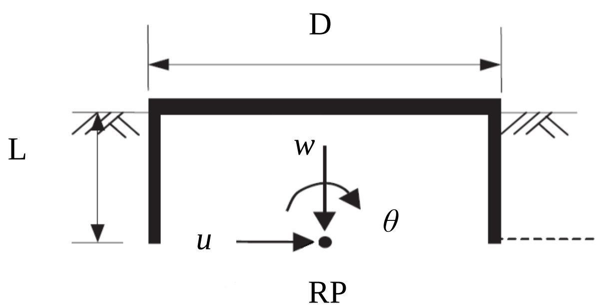

Figure 2: Foundation geometry

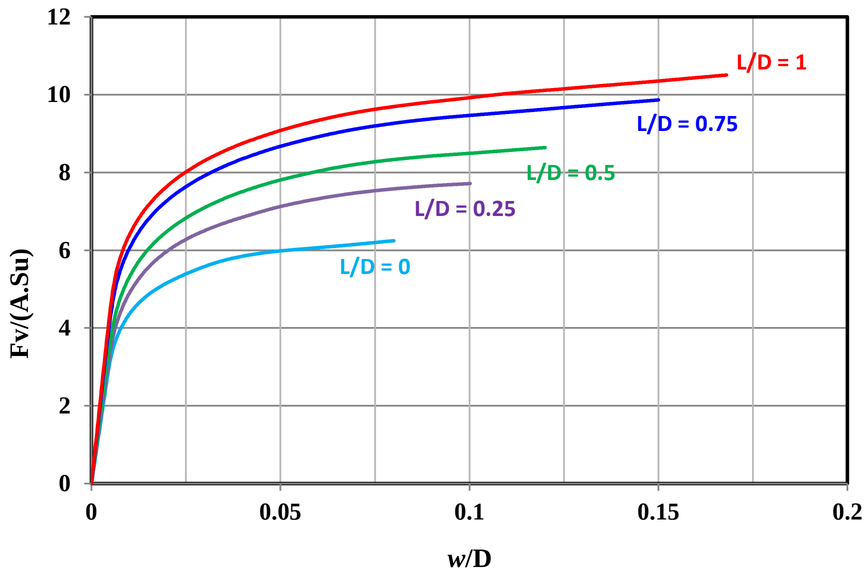

Figure 3: Normalised vertical load for different embedment ratios (L/D) vs normalised vertical displacement (w/D)

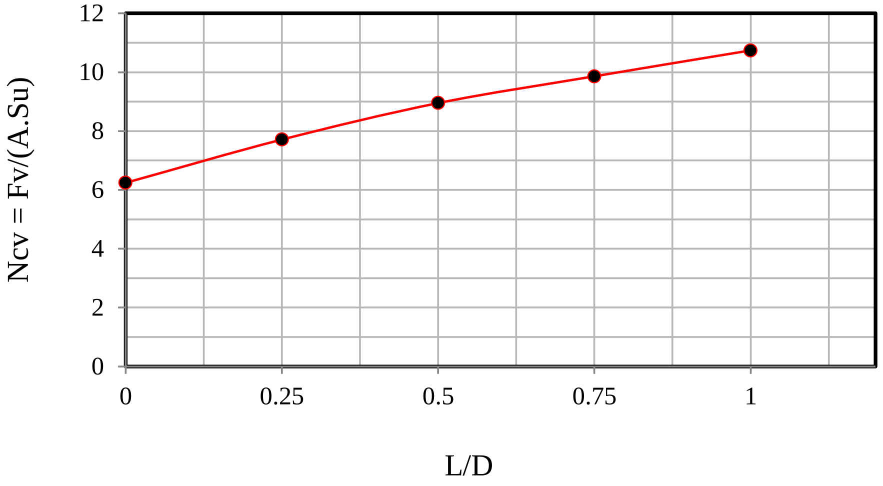

Figure 4: Vertical bearing capacity factor as a function of embedment ratio

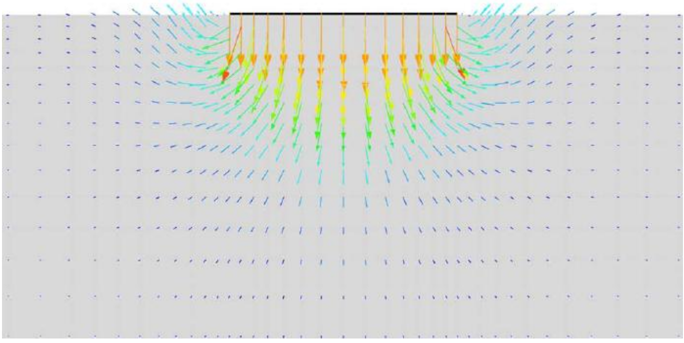

(a)

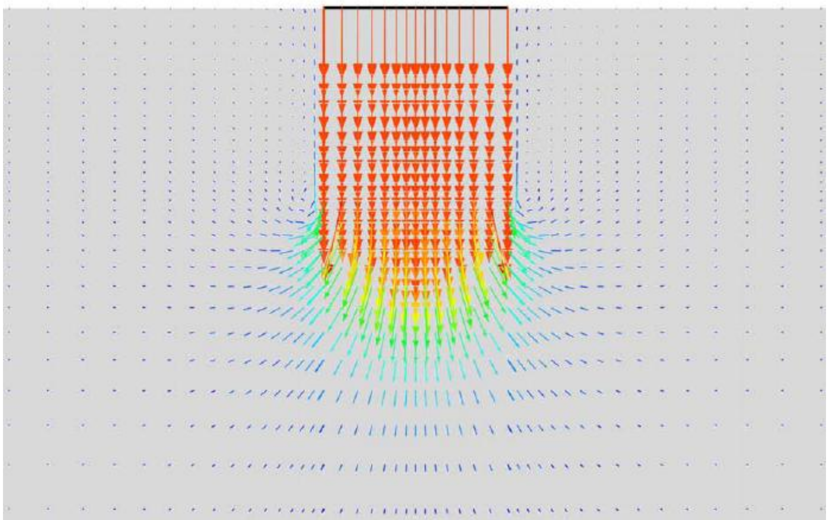

(b)

Figure 5 (a-b): Failure mechanism under vertical load, (a) L/D=0 (surface foundation), (b) L/D=1

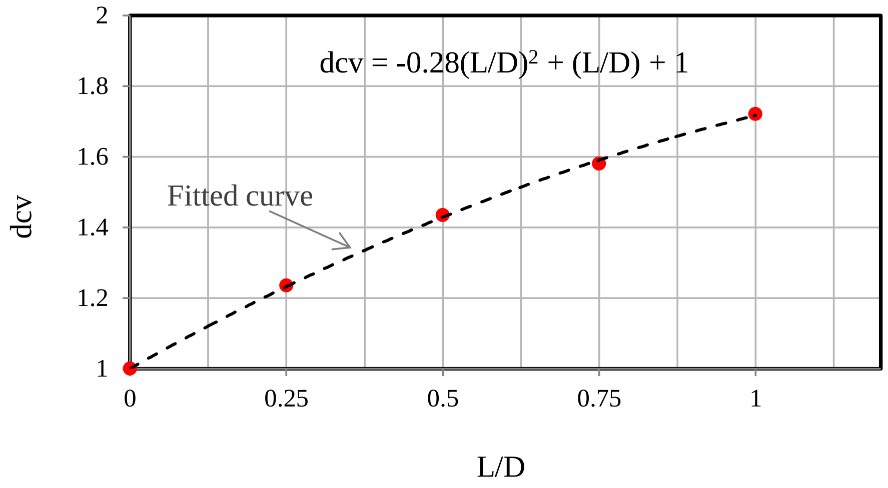

Figure 6: Vertical depth factor as a function of L/D ratios

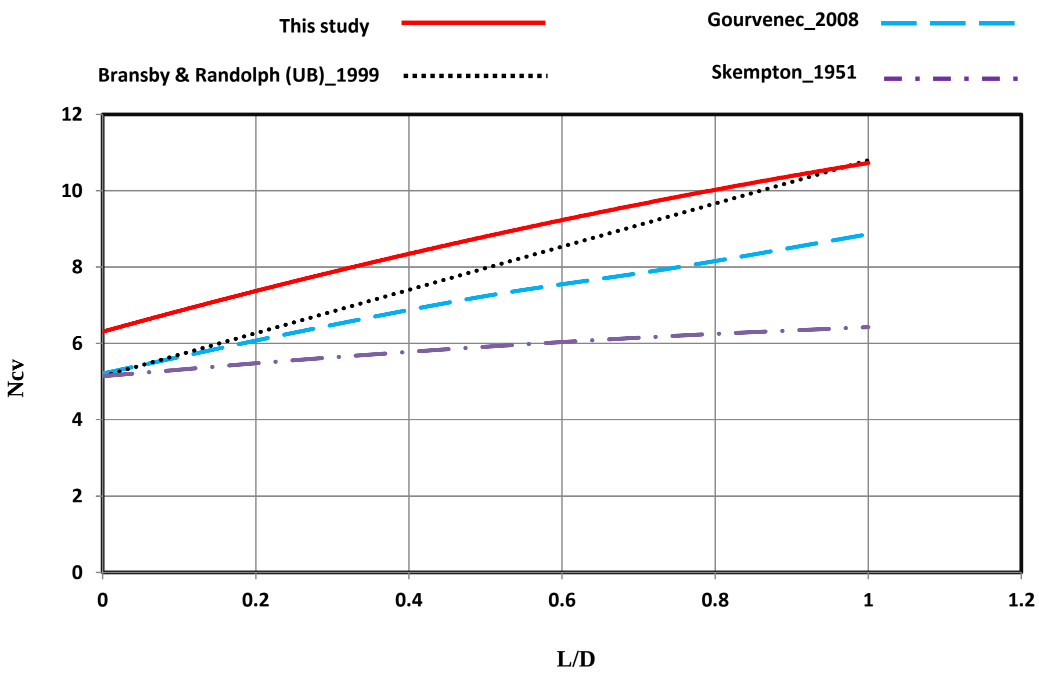

Figure 7: Comparison of vertical bearing capacity

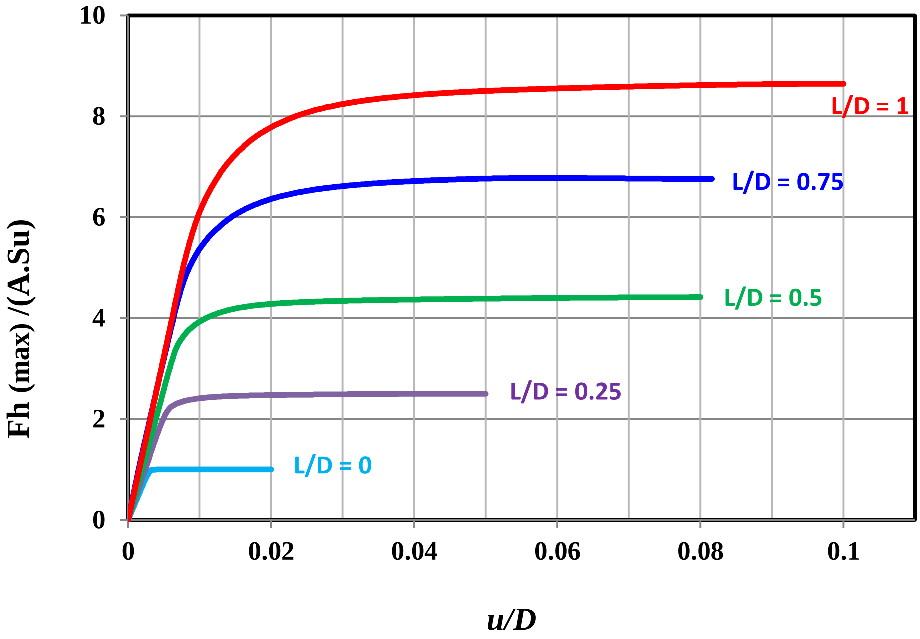

Figure 8: Normalised horizontal load for different embedment ratios (L/D) vs normalised horizontal displacement (u/D)

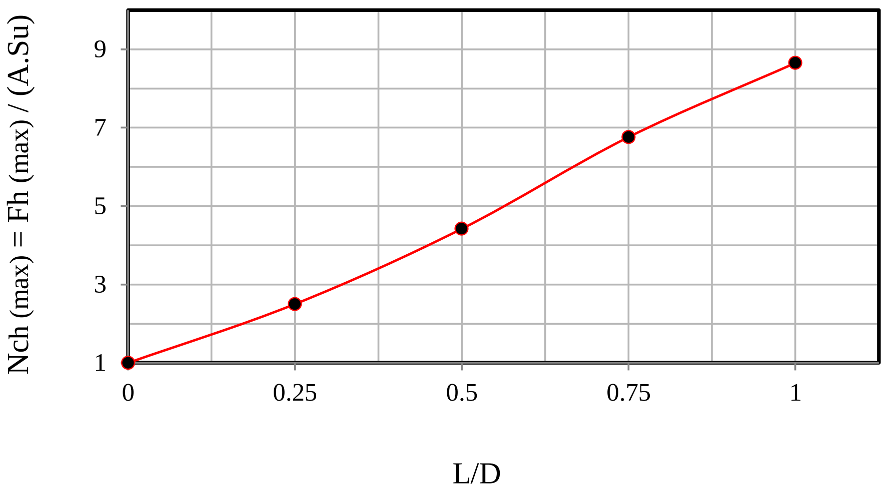

Figure 9: Maximum horizontal bearing capacity as a function of embedment ratio

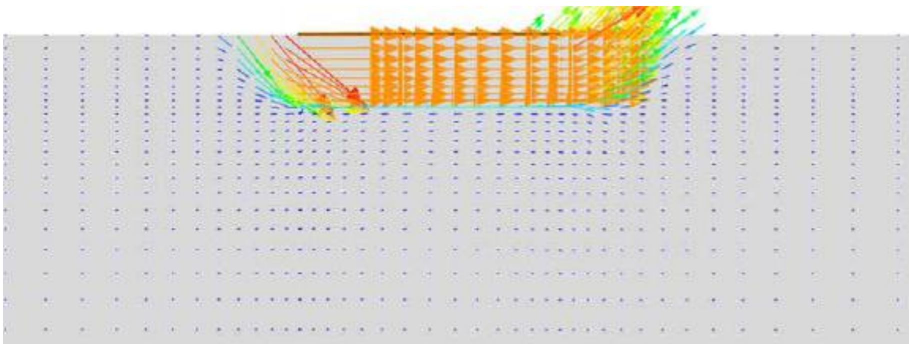

(a)

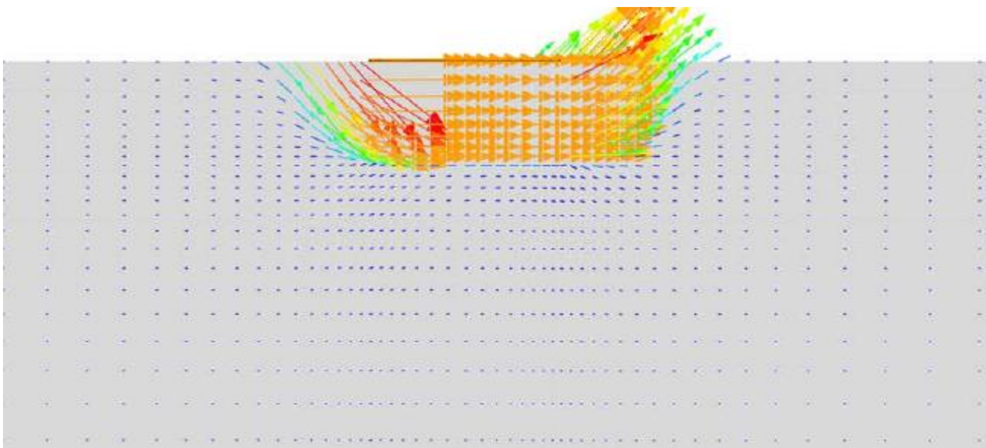

(b)

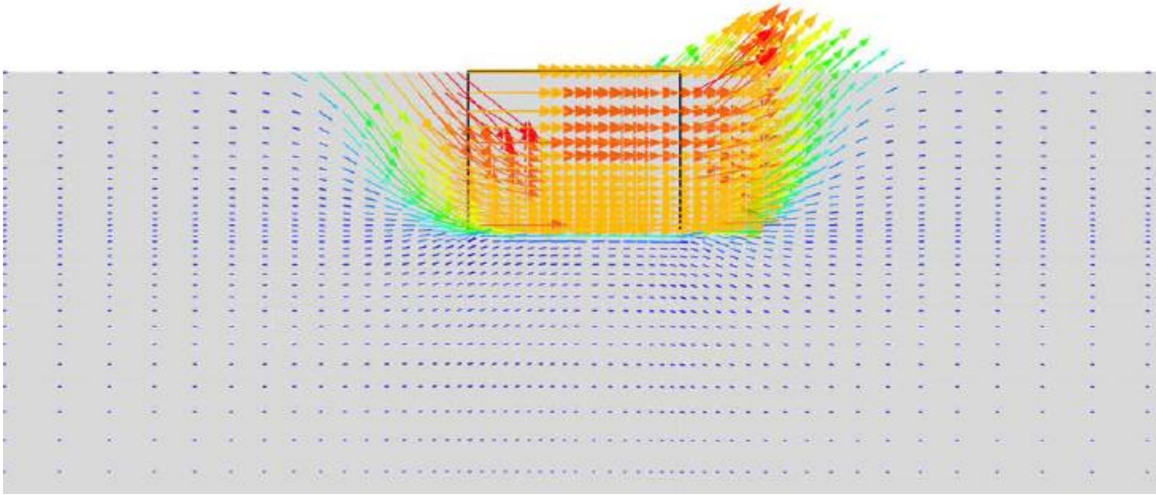

(c)

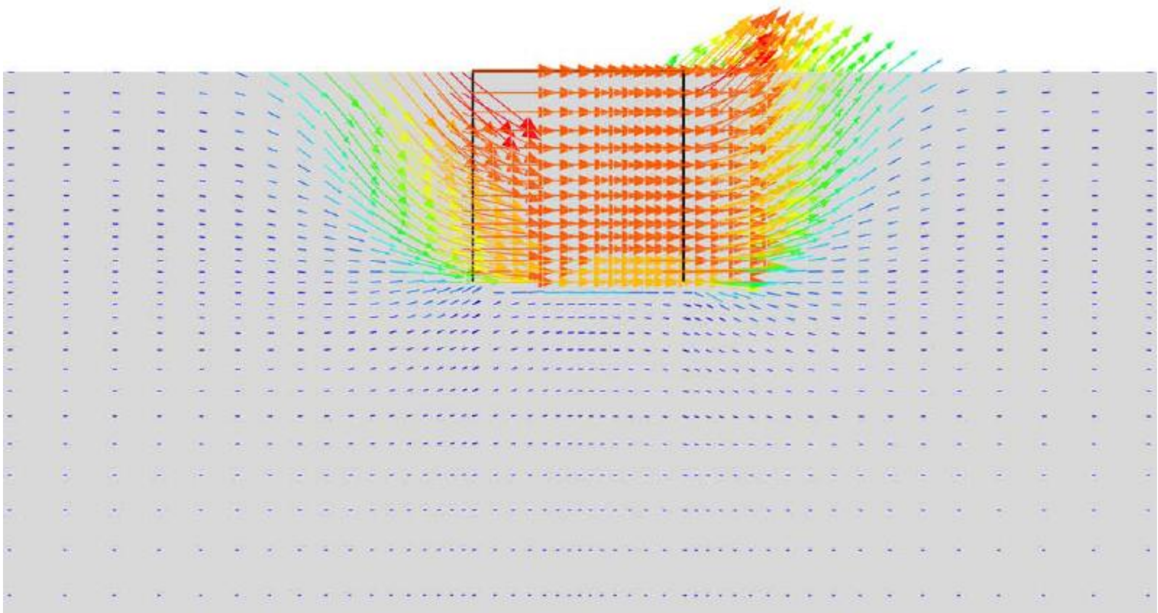

(d)

Figure 10(a-d): Failure mechanism under horizontal load (h $_{max;}$ θ constrained), (a) *L*/D=0.25, (b) *L*/D=0.5, (c) *L*/D=0.75, (d) *L*/D=1

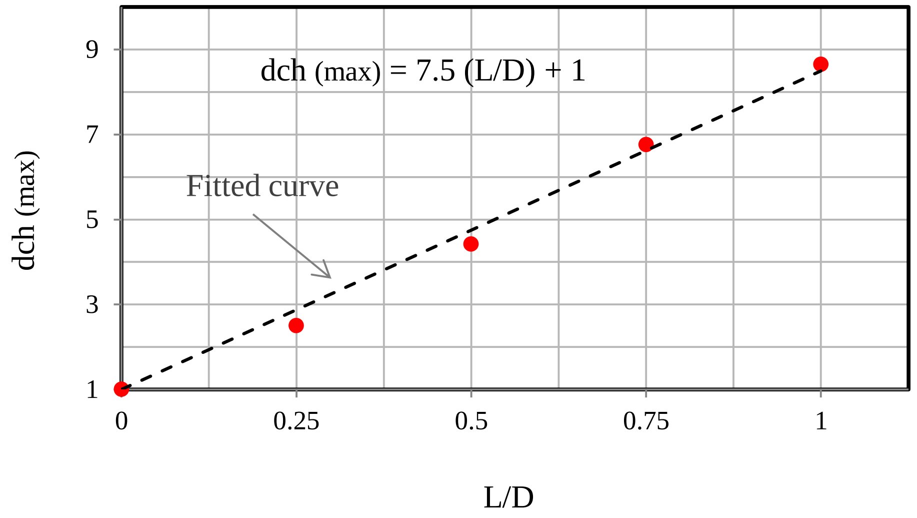

Figure 11: Maximum horizontal capacity depth factor as a function of *L*/D ratios

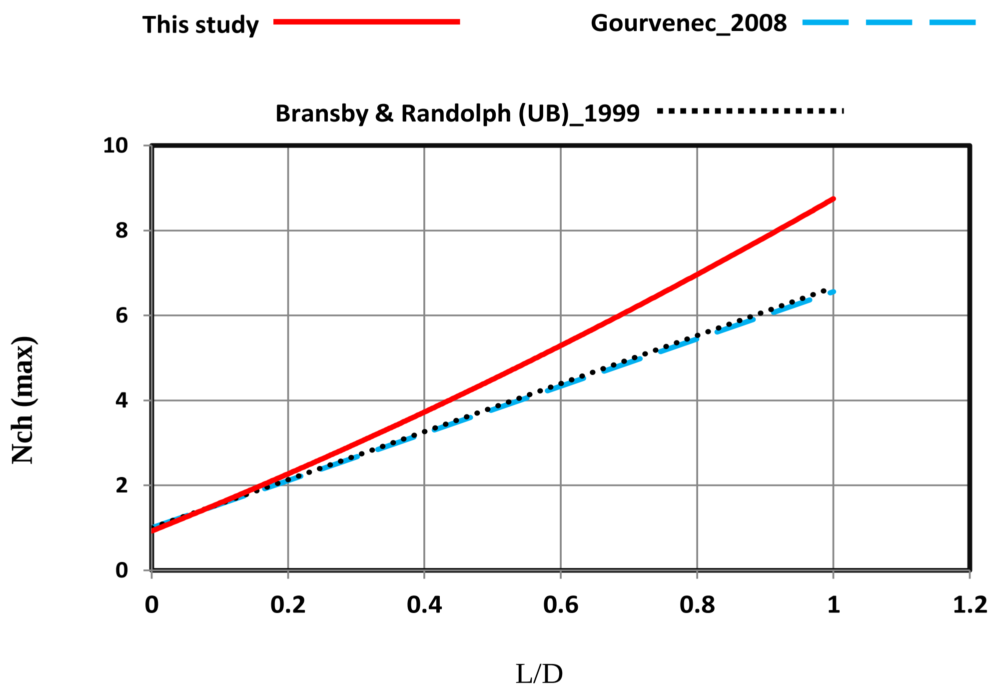

Figure 12: comparison of maximum horizontal bearing capacity predictions

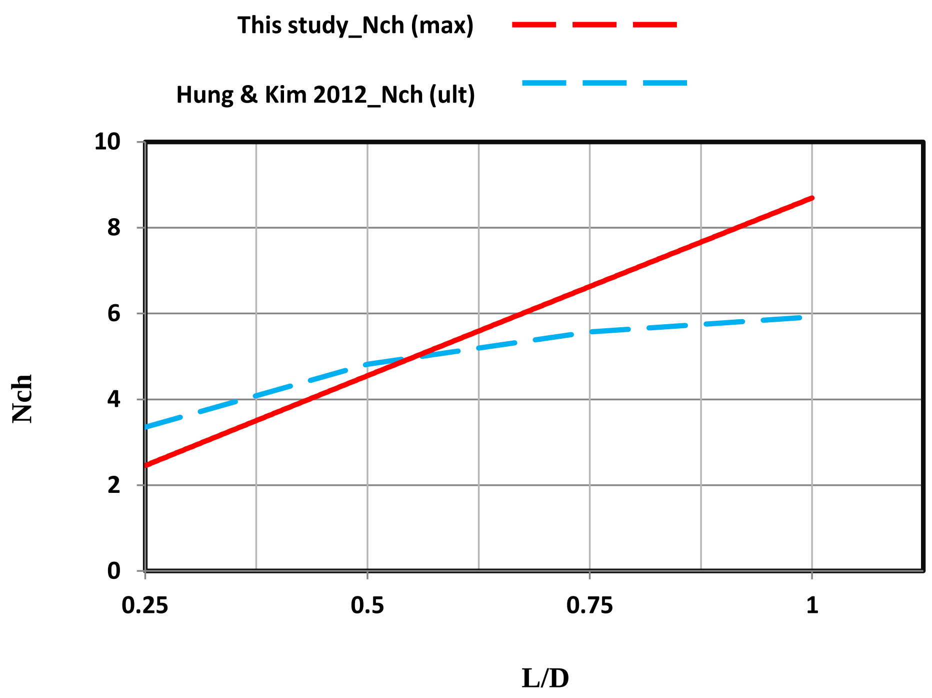

Figure 13: A comparison between ultimate and maximum horizontal bearing capacity factors; $N_{ch\ (ult)}$ & $N_{ch\ (max)}$ when θ *is* constrained

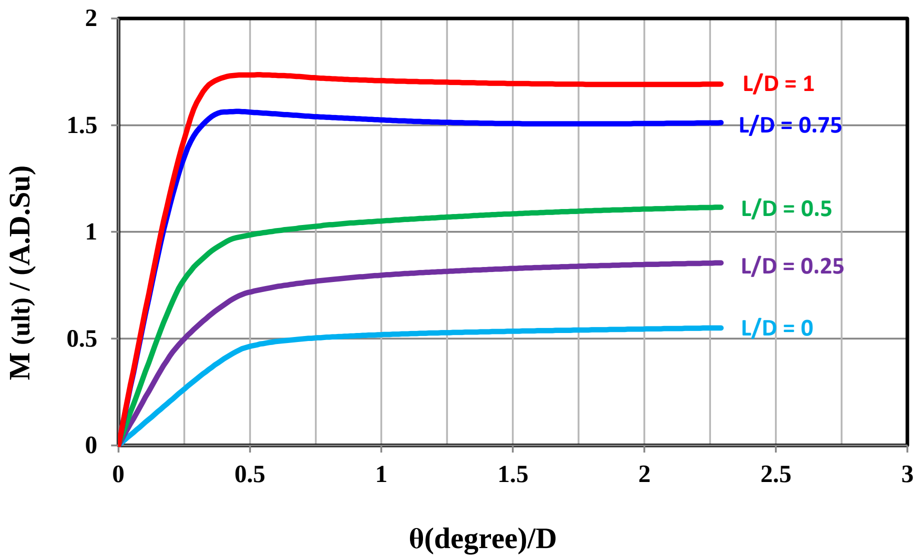

Figure 14: Normalised moment for different embedment ratios (*L*/D) vs normalised rotation (*θ*/D)

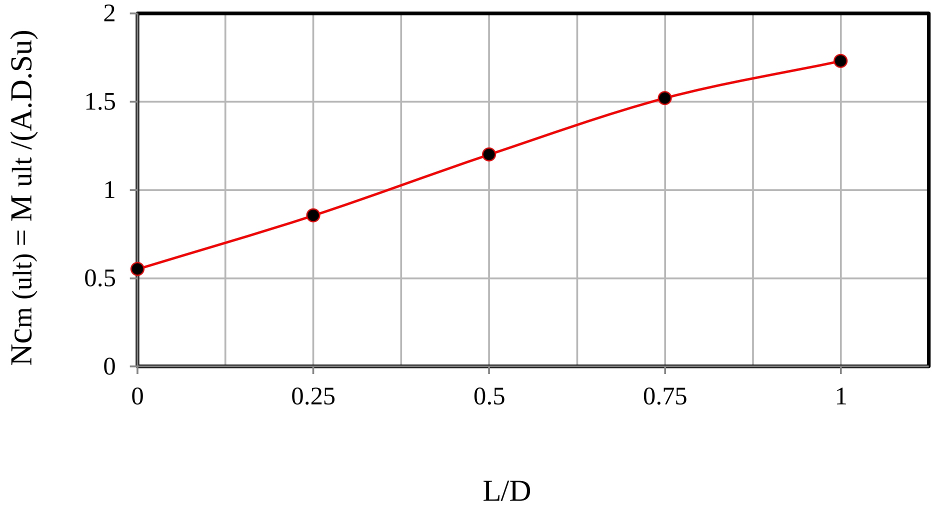

Figure 15: Ultimate moment capacity as a function of embedment ratio

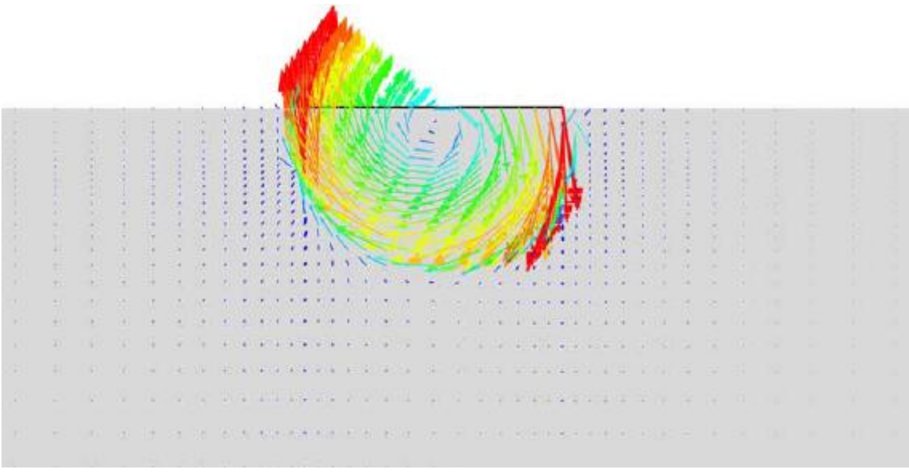

(a)

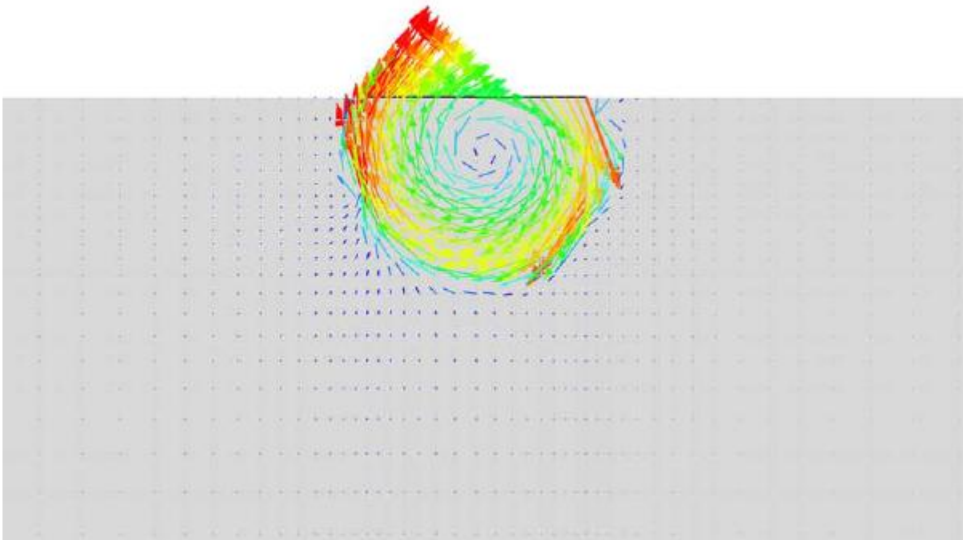

(b)

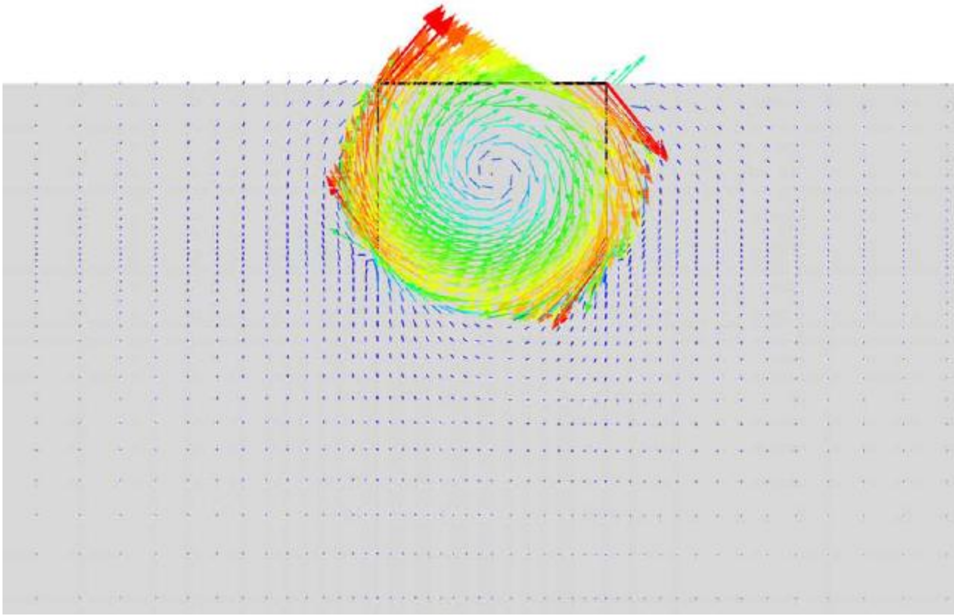

(c)

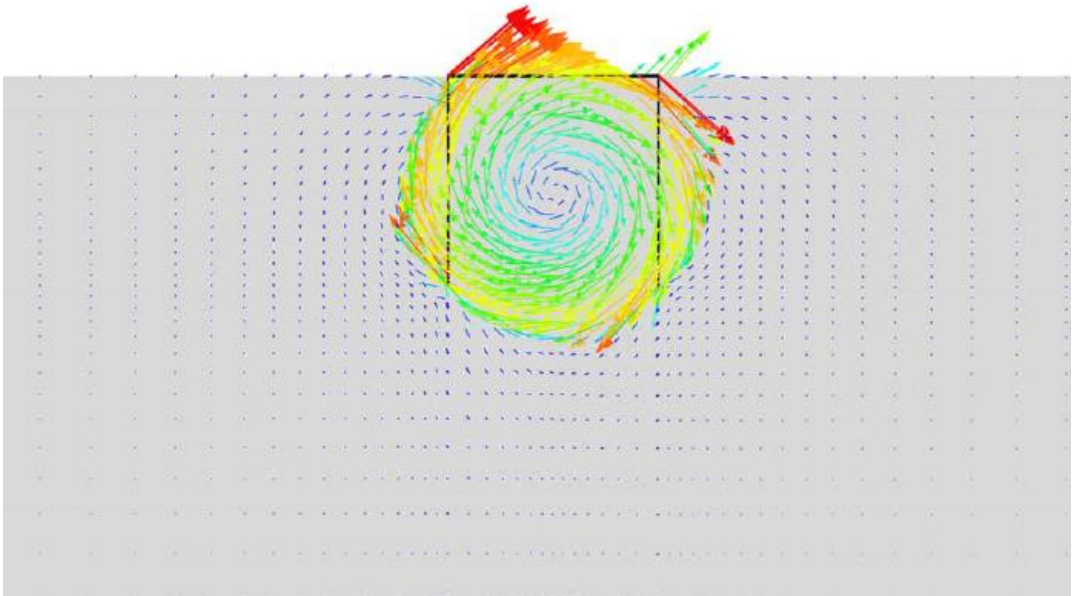

(d)

Figure 16 (a-d): Failure mechanism under moment load (M_{ult}; *u* is not constrained), (a) *L*/D=0.25, (b) *L*/D=0.5, (c) *L*/D=0.75, (d) *L*/D=1

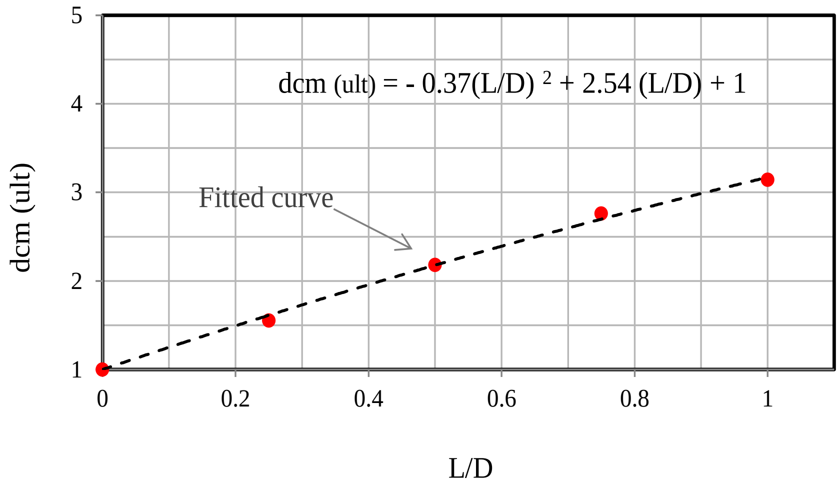

Figure 17: Ultimate moment capacity depth factor as a function of L/D ratios

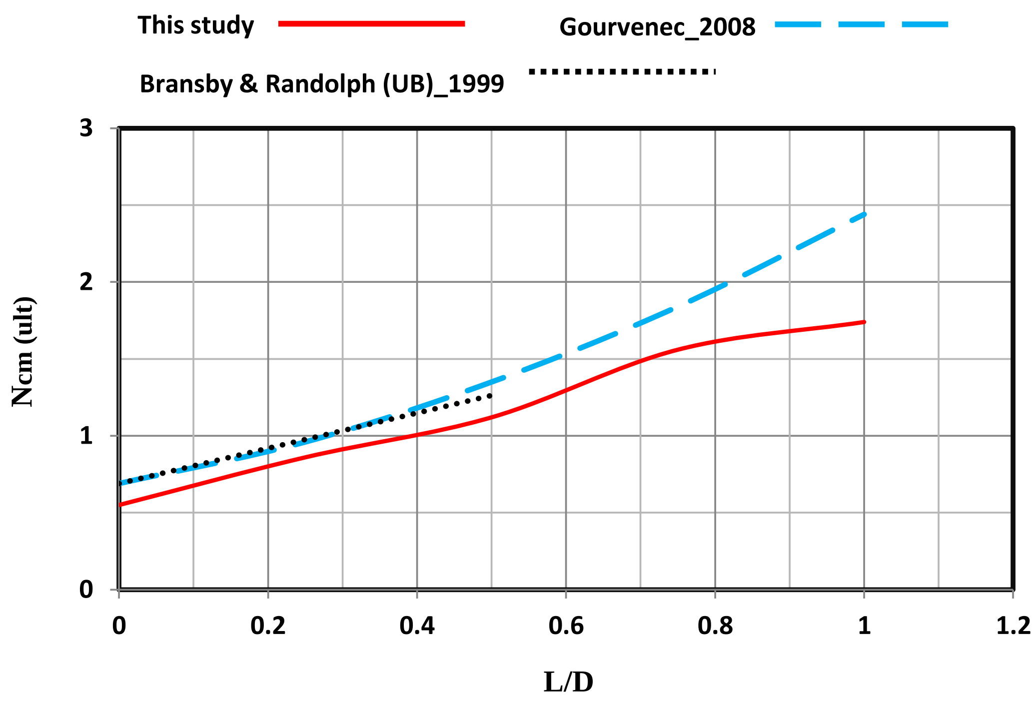

Figure 18: Comparison of ultimate moment bearing capacity factor

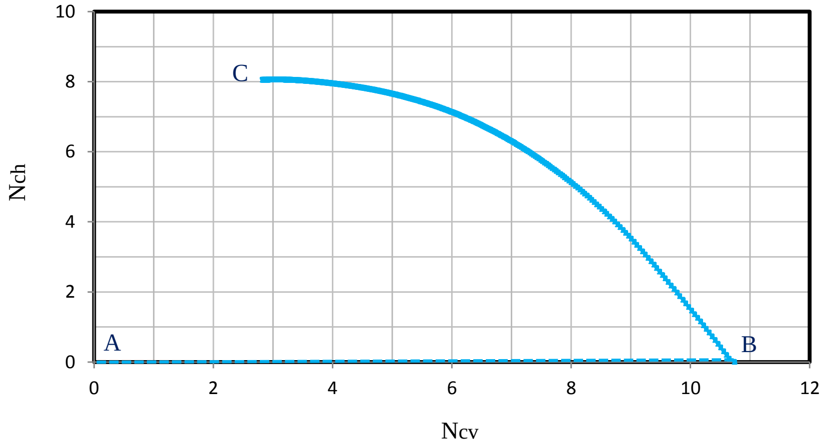

Figure 19: A cross section of yield locus in V-H space using side-swipe method

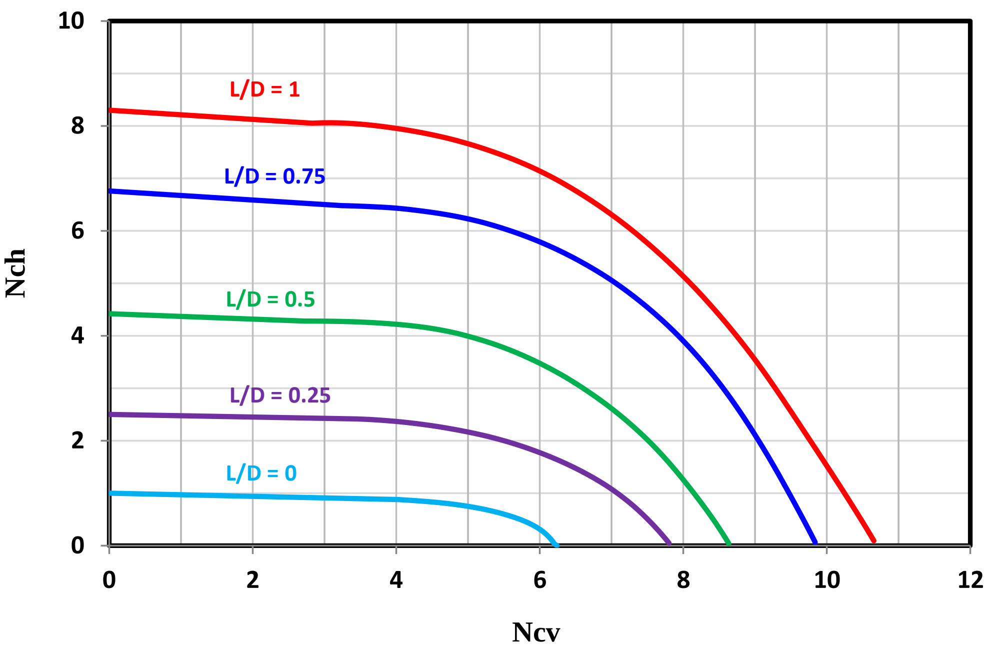

Figure 20: Failure envelopes for vertical and horizontal loading space (moment load = 0)

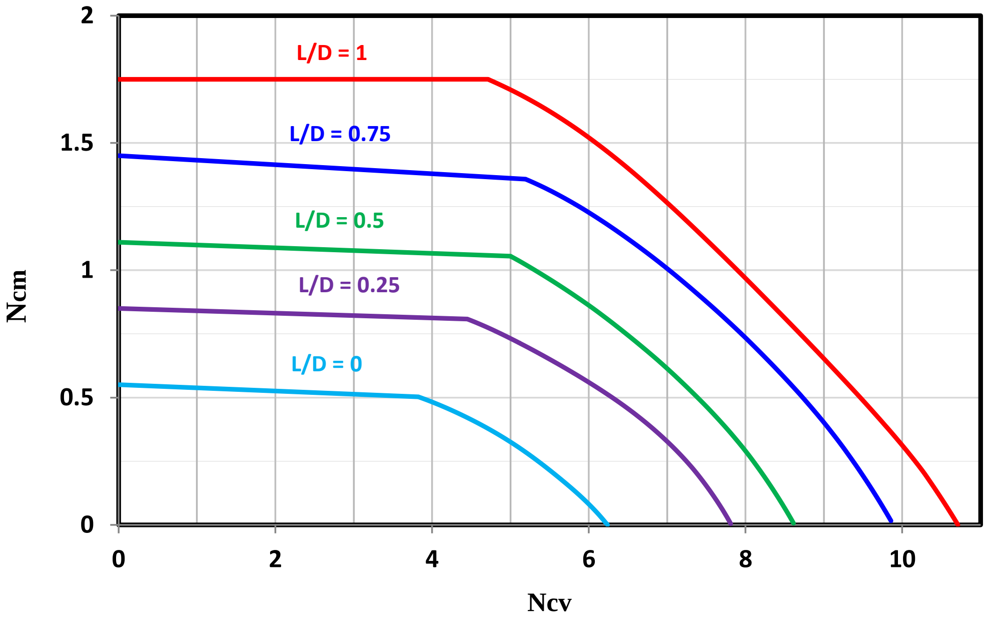

Figure 21: Failure envelopes for vertical and moment loading space (horizontal load = 0)